PNAS RESEARCH ARTICLE | APPLIED BIOLOGICAL SCIENCES

Implanted synthetic cells trigger tissue angiogenesis through de novo production of recombinant growth factors

Gal Chen[a,b], Rotem Levin[a], Shira Landau[c], Maya Kaduri[a], Omer Adir[a,d], Iris Ianovici[c], Nitzan Krinsky[a], Ofri Doppelt-Flikshtain[a,e], Jeny Shklover[a], Janna Shainsky-Roitman[a], Shulamit Levenberg[c], and Avi Schroeder[a,1]

Edited by Joseph DeSimone, Stanford University, Stanford, CA; received May 9, 2022; accepted August 12, 2022

Progress in bottom-up synthetic biology has stimulated the development of synthetic cells (SCs), autonomous protein-manufacturing particles, as dynamic biomimetics for replacing diseased natural cells and addressing medical needs. Here, we report that SCs genetically encoded to produce proangiogenic factors triggered the physiological process of neovascularization in mice. The SCs were constructed of giant lipid vesicles and were optimized to facilitate enhanced protein production. When introduced with the appropriate genetic code, the SCs synthesized a recombinant human basic fibroblast growth factor (bFGF), reaching expression levels of up to $9{\cdot}10^6$ protein copies per SC. In culture, the SCs induced endothelial cell proliferation, migration, tube formation, and angiogenesis-related intracellular signaling, confirming their proangiogenic activity. Integrating the SCs with bioengineered constructs bearing endothelial cells promoted the remodeling of mature vascular networks, supported by a collagen-IV basement membrane–like matrix. In vivo, prolonged local administration of the SCs in mice triggered the infiltration of blood vessels into implanted Matrigel plugs without recorded systemic immunogenicity. These findings emphasize the potential of SCs as therapeutic platforms for activating physiological processes by autonomously producing biological drugs inside the body.

artificial cells | cell-free | tissue engineering | angiogenesis | targeted drug delivery

Bottom-up engineered synthetic cells (SCs) are designed to portray some similar features of natural cells, as well as unique properties developed for artificial nonliving systems (1). Gene expression, spatial organization, DNA replication, and communication are only a few examples of cell functionalities integrated into these synthetic systems (2–7). Owing to their modularity and programmability, SCs have become a focus of interest for their potential use in biomedical applications—notably, as complementary technologies in cell therapy and as sophisticated biomimetic drug delivery platforms (8–10).

SCs have been shown to trigger cellular processes by their autonomous chemical interaction with natural cells (11). Examples include genetically encoded SCs that guide the differentiation of neuronal stem cells and SCs that promote glucose uptake in breast cancer cells (3, 12). In addition, toxin-producing SCs, administered to breast cancer–bearing mice, resulted in tumor cell apoptosis (13). However, utilizing SCs for inducing multistage biogenesis processes at a physiological level in the dynamic environment of living tissue has not been explored yet. Angiogenesis, the multistage process of forming new blood vessels from preexisting capillaries, can serve as a model for studying these capabilities of SCs. Angiogenesis is a prerequisite for proper organ implantation, tissue regeneration, and healing (14, 15). In this regard, SCs enabling the on-site production of growth factors can potentially address the need for the continuous delivery and secretion of growth factors during the tissue remodeling process (16).

Here, we describe the engineering of proangiogenic SCs that were genetically encoded to secrete a recombinant human basic fibroblast growth factor (bFGF) that biochemically signals to endothelial cells in vitro and in vivo. The SCs were composed of giant unilamellar lipid vesicles (GUVs; >1 μm) loaded with a cell-free protein synthesis (CFPS) system designed to express the proangiogenic factor (Fig. 1*A*). The membrane lipid composition of the SCs was optimized to allow functional CFPS encapsulation and soluble protein production capacity. The proangiogenic SCs were then cocultured with human umbilical vein endothelial cells (HUVECs) to promote angiogenesis-associated cell signaling, starting from cell proliferation to the formation of stabilized vascular networks. Finally, SCs injected within a Matrigel matrix in mice triggered the infiltration of new blood capillaries. By this method, we have demonstrated how protein-producing SCs can stimulate a natural, multistage physiological process in live tissue. This study presents the potential of bioengineered SCs to support cellular processes of tissue regeneration and healing inside the body.

Significance

Synthetic cells, artificial cell-like particles, were engineered using synthetic biology tools to produce therapeutic proteins inside the body. Synthetic biology promises to overcome malfunctioning natural processes and treat disease. This study designed synthetic cells that produce recombinant growth factors to support angiogenesis and tissue regeneration. The synthetic cells triggered the self-organization of natural capillary networks and recruited blood vessels to tissue grafts in mice. The body tolerated the synthetic cells well for prolonged periods of time without eliciting a systemic immune response. Integrating synthetic cells within the body expands biomedical capabilities and can address a multitude of conditions beyond natural capabilities.

Author contributions: G.C., R.L., S.L., M.K., O.A., I.I., N.K., O.D.-F., and A.S. designed research; G.C., R.L., S.L., M.K., O.A., I.I., and O.D.-F. performed research; S.L. contributed new reagents/analytic tools; G.C., R.L., S.L., M.K., O.A., I.I., O.D.-F., J.S., and J.S.-R. analyzed data; and G.C. and A.S. wrote the paper.

The authors declare no competing interest.

This article is a PNAS Direct Submission.

[1]To whom correspondence may be addressed. Email: avids@technion.ac.il.

This article contains supporting information online at http://www.pnas.org/lookup/suppl/doi:10.1073/pnas.2207525119/-/DCSupplemental.

Published September 12, 2022.

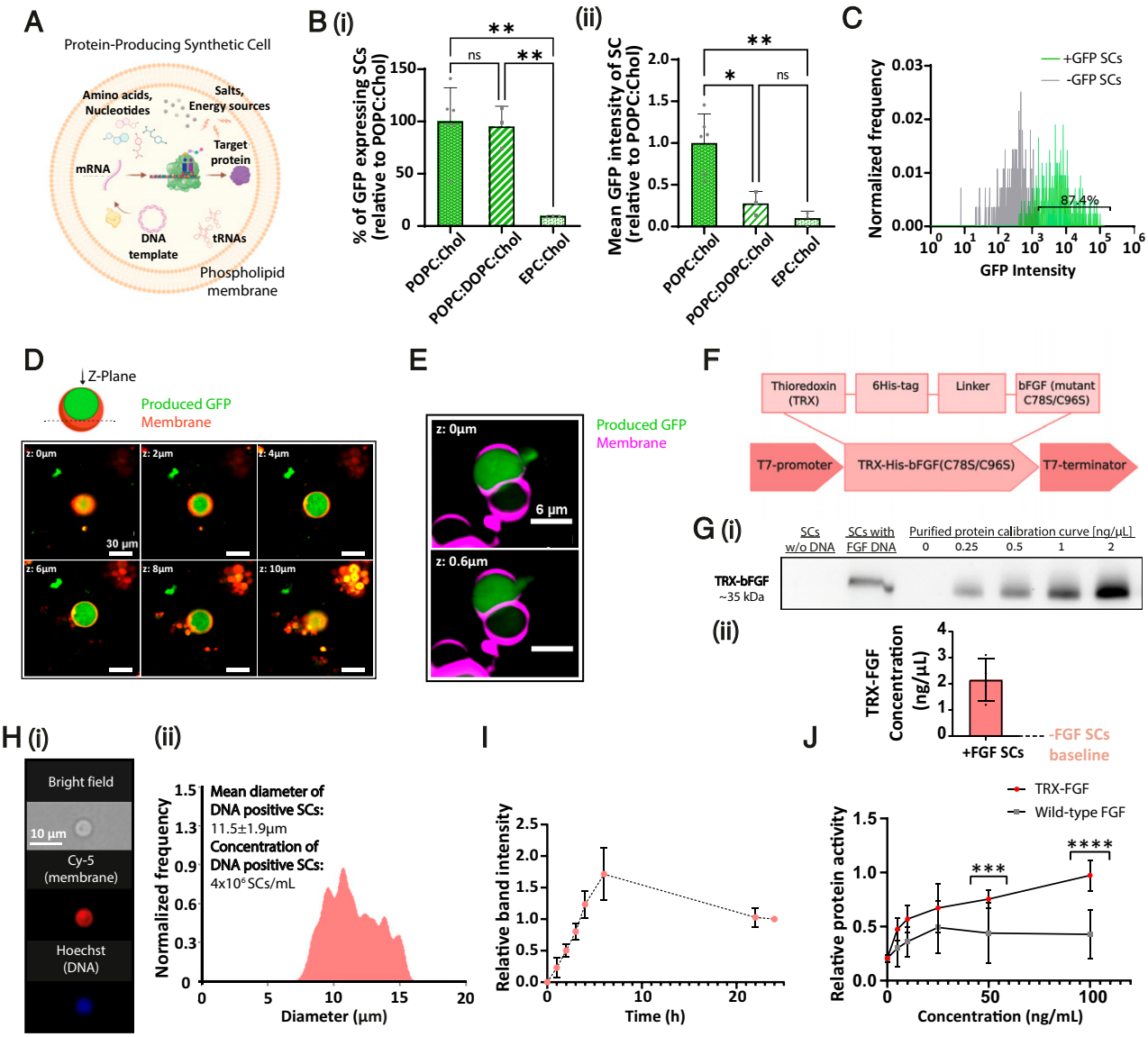

Fig. 1. Engineering proangiogenic SCs. (*A*) Schematic illustration of a protein-producing SC. (*B*) The effect of lipid composition on SC activity (protein production). (*i*) Percentage of GFP-expressing SCs in different formulations. (*ii*) Mean fluorescence intensity per SC (mean GFP production) of the examined formulations. All values were normalized to POPC:Chol formulation. Chol, cholesterol. Data represent mean ± SD (n = between 3 and 6). One-way ANOVA with adjusted P value in multiple comparisons tests; *P = 0.0113; **$P \leq 0.0071$. (*C*) Percentage of protein-producing SCs in POPC:Chol–based cells. (*D*) Representative images of GFP-producing SCs in 2-µm scan depth gaps (z-plane); produced GFP (in green), Cy-5–labeled membrane (in red). Scale bar, 30 µm. (*E*) Detection of GFP release from an SC. Cy-5–labeled (purple) and GFP (green)-producing SCs were monitored under spinning-disk confocal microscopy. Images of a single GFP-expressing SC in 0.6-µm z-plane gaps show protein release in a specific spot of the SC membrane. (*F*) Schematic of the different elements in the fusion TRX–human bFGF protein sequence. (*G*) (*i* and *ii*) Western blot quantification of TRX-FGF production in SCs after 3 h of incubation (37 °C), based on purified TRX-FGF protein calibration curve (n = 4). Data represent mean ± SD. (*H*) Imaging flow cytometry characterization of FGF-producing SCs. (*i*) SCs were fabricated with Cy-5–conjugated lipid (red) incorporated in their membrane and stained using Hoechst DNA dye (blue). (*ii*) Mean diameter histogram of DNA-positive SCs (blue+red+) and their concentration. (*I*) Production kinetics of TRX-FGF in SCs at 37 °C over 24 h. Samples of each gel were normalized to their corresponding 24-h sample (= 1), (n = 3). For data analysis, n represents the number of independent samples from each group. Data represent mean ± SD. (*J*) Purified TRX-FGF shows higher protein activity than a native basic FGF. Protein activity was evaluated by inducing primary HUVEC proliferation in different concentrations [ng/mL]. Values were normalized to 100 ng/mL of TRX-FGF treatment. Data represent mean ± SD (n = 13). Unpaired two-tailed t test P value; ***P = 0.0002; ****$P < 0.0001$. mRNA, messenger RNA; ns, not significant; tRNA, transfer RNA; w/o, without.

Results

Membrane Lipid Composition Affects SC Activity. The lipid bilayer, composing the cellular envelope, affects cell stability and permeability (17). We showed that the lipid composition of the SC affects its protein production efficiency. We screened 10 different phosphatidylcholine (PC)-based SC formulations, prepared using the water/oil emulsion transfer method (*SI Appendix*, Tables S1 and S2) (18). The phospholipids used to construct the membrane varied in their fatty acid chain length and saturation degree, ranging from 14:0 to 18:1 hydrocarbon tails. All formulations were supplemented with different amounts of cholesterol to enhance membrane stability (19). Only three of the screened formulations self-assembled into viable GUVs under the formulation conditions—1-palmitoyl-2-oleoyl-glycero-3-phosphocholine (POPC):Cholesterol (1:1), POPC:1,2-diole, oyl-sn-glycero-3-phosphocholine (DOPC):Cholesterol (4:3:1), and Egg-PC (EPC):Cholesterol (1:1) weight ratios (*SI Appendix*, Fig. S1).

To test SC activity, we incorporated a CFPS system (based on *Escherichia coli* S30-T7 cell extract) and a green fluorescence protein (GFP)–reporter DNA template into the SCs. We quantified protein production inside the vesicles by measuring their

resultant fluorescent signal. The percentage of GFP-expressing SCs, indicating the encapsulation of a functional CFPS system, and the mean fluorescence intensity per SC, demonstrating its protein expression capabilities, were examined for each membranal formulation. Both values were highest for POPC-based formulations compared to POPC:DOPC or EPC-based SCs (Fig. 1 *B*, *i* and *ii*). Based on these findings, a POPC-based composition generating the most efficient SCs was used next in this study. These experiments were also repeated using a PURE (protein synthesis using recombinant elements) system (20) loaded into the SCs, retrieving similar results (*SI Appendix*, Fig. S2).

Imaging flow cytometry was used to analyze the percentage of active protein-producing SCs within the total SC population. As the SCs were intended for in vivo applications, their inner content was derived from this point using a PURE system to ensure less immunogenic administration. The water/oil emulsion method, selected for its high encapsulation efficiency (21), produced above 87% active SCs (Fig. 1*C*). Representative confocal images of GFP-producing SCs through the z-plane demonstrated protein expression surrounded by the rhodamine-labeled lipid membrane (Fig. 1*D*).

To study the release profile of proteins from SCs and SC stability under physiological conditions, we synthesized SCs with a Cy5 fluorescent label in the membrane and DNA encoded to express GFP internally. Spinning-disk confocal microscopy elucidated that internally produced GFP was released from the SC due to membrane rupture (Fig. 1*E*). This finding was supported by a decline in GFP fluorescence levels in the SCs over time. In addition, measurements of SC size over 24 h did not show a significant change during the experiment, suggesting that micro tears or ruptures in the lipid membrane, rather than SC fusion or disruption, allowed protein release from SCs (*SI Appendix*, Fig. S3). This result may be explained by the soft lipid shell these SCs have at physiological temperature, which helps facilitate protein release.

Engineering Proangiogenic SCs. POPC-based SCs were encoded to produce human bFGF. Similar to vascular endothelial growth factor (VEGF), bFGF is a potent key angiogenic inducer both in vitro and in vivo and is highly conserved between humans and other species (22–24). The extracellular activity of bFGF, mediated by the conserved transmembrane tyrosine kinase receptors Fibroblast growth factor receptors (FGFRs), made it suitable for application through synthesis and release by SCs (25). To allow the expression of human bFGF in a bacterial-based expression system, the gene sequence of the protein was optimized according to the codon preference of *E. coli* to reflect the codon usage of the host without modifying the encoded protein sequence. The gene sequence was then introduced with two site-direct mutations to increase the protein mitogenic activity, replacing cysteines 78 and 96 with serines (26). Furthermore, a Thioredoxin (TRX) tag, which has been shown to increase protein solubility (27), was fused to the N-terminal end and linked to a 6-Histidine (His) tag that was inserted to allow protein purification (Fig. 1*F*; the full gene map is presented in *SI Appendix*, Table S3). The synthetic DNA insert was integrated under T7 promoter and terminator control to allow protein overexpression at physiological temperature. Next, we incorporated the TRX-bFGF DNA template into the SCs with a PURE expression system adjusted to enable the formation of SCs through emulsion transfer (*SI Appendix*, Fig. S4). Incubating the SCs under physiological conditions for 3 h led to an average protein production concentration of 2.15 ± 0.8 ng/μL, as quantified by Western blot, using an anti-bFGF antibody (Fig. 1*G* and *SI Appendix*, Fig. S5*A*). Comparing the estimated practical reaction volume produced by SCs to the cell-free bulk reaction demonstrated at least 4.9-fold higher fibroblast growth factor (FGF) production yields in SCs compared to a nonencapsulated system (*SI Appendix*, Fig. S5*B* and Eq. **S1**). This result, also supported by previous studies (13, 28), highlights the importance of the molecular crowding effect and compartmentalization of metabolic reactions evolved in nature. Next, we used imaging flow cytometry to determine the morphology, size distribution, and concentration of FGF DNA containing SCs (Fig. 1*H*). The mean SC diameter measured was 11.5 ± 1.9 μm with $4{\cdot}10^6$ SCs/mL concentration. Crossing Western blot total concentration data with SC concentration measurements implied an average of 0.54 pg FGF per single SC, which corresponds to $9{\cdot}10^6$ protein copies. Moreover, we studied the production kinetics in SCs over 24 h using quantitative immunoblotting. Although sufficient growth factor levels for physiological application were quantified after 3 h, the reaction kept its dynamic production for at least 6 h (Fig. 1*I*). To test the biological activity of the synthesized recombinant protein, we purified the TRX-bFGF protein from BL21(DE3) bacterial cells (*SI Appendix*, Fig. S6) and compared its activity to a commercial wild-type bFGF. The mutant TRX-bFGF showed dose-dependent activity and significantly better ability to stimulate endothelial cells than the wild-type form (Fig. 1*J*).

FGF-Producing SCs Induce HUVEC Proliferation. Activation of endothelial cell proliferation by FGF has been associated with stimulation of the RAS-mitogen-activated protein kinase (MAPK) signaling pathway, usually evaluated by the phosphorylation of the extracellular regulated protein kinases 1/2 (ERK1/2) (25, 29). To study the proangiogenic activity of FGF-producing SCs, we first tested their mitogenicity. Applying both purified and cell-free–produced FGF (FGF CF; SCs' inner content) to primary HUVECs resulted in a significantly higher phospho-ERK (pERK)/total ERK ratio compared to the cell-free reaction without DNA or to the untreated cell controls (Fig. 2*A*). To further confirm the mitogenic effect of the SCs on HUVECs, we performed metabolic and microscopic-based assays over 48 h (Fig. 2 *B*, *i*). Cells treated with SCs without DNA templates (non–protein-producing) and untreated cells served as controls. Cell proliferation was increased following incubation of the culture with FGF-producing SCs compared to controls (Fig. 2 *B*, *ii* and *iii*). These findings were corroborated using confocal microscopy (Fig. 2 *B*, *iv*). These results confirm the engineering of biologically active SCs that biochemically induced the proliferation of endothelial cells through FGF release.

FGF-Producing SCs Guide the Formation of EC Capillaries. We utilized an in vitro capillary-like formation setup to investigate the proangiogenic potential of SCs. In vitro formation of capillary-like structures by endothelial cells indicates the activation of multiple angiogenic steps (e.g., cell adhesion, migration, alignment, and tubule formation) (30). Briefly, GFP-expressing HUVECs were seeded on a reduced–growth factor basement-membrane matrix in starvation media and incubated with or without SCs for 18 h. Time-lapse images of the process in 1-h gaps were acquired (Movie S1), and images of the assay peak were analyzed using the AngioTool software (31). Treatment with FGF-producing SCs resulted in significantly higher average vessel length in the formed network compared to the controls (Fig. 2 *C*, *i* and *ii* and *SI Appendix*, Fig. S8). These data

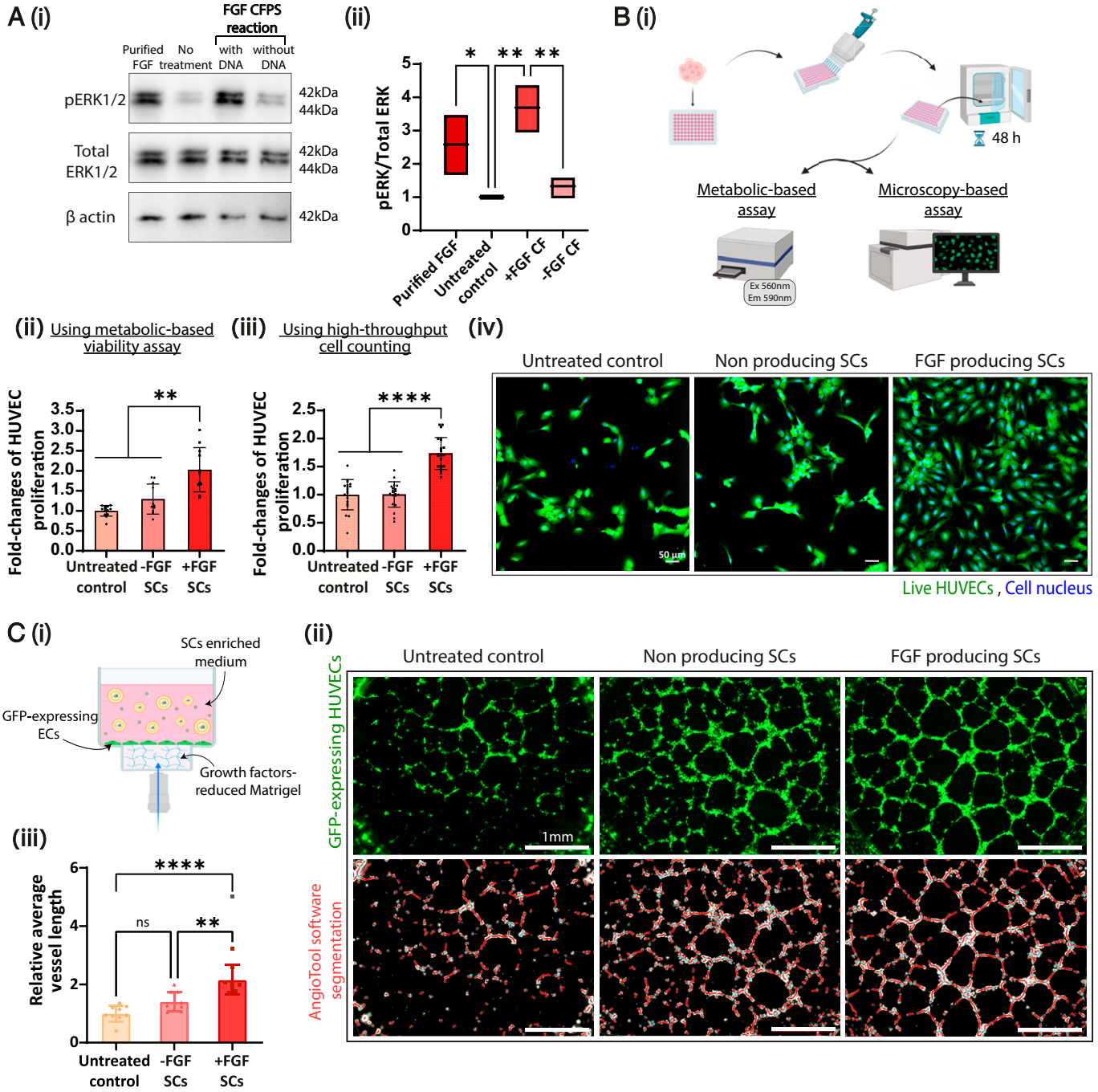

Fig. 2. Proangiogenic SCs induce endothelial cell proliferation and tube formation. (*A*) (*i*) Higher expression of pERK in HUVECs in response to a cell-free–produced FGF treatment (+FGF CF) compared to a cell-free reaction without DNA (−FGF CF); purified FGF and untreated cells are displayed in Western blot images. (*ii*) Band area quantification of pERK/total ERK values normalized to untreated control ($n = 3$). Floating bars represent min to max and mean values; $^{*}P = 0.0453$, $^{**}P \leq 0.0054$. (*B*) (*i*) HUVECs were treated with SCs prepared with/without inclusion of the TRX-bFGF DNA vector (+/−FGF SCs, respectively). Increased cell proliferation was detected in +FGF SC treatment after 48 h using (*ii*) viability assay and (iii) cell nuclei counting. All treatments were normalized to untreated control(n = between 11 and 20). $^{**}P \leq 0.0055$; $^{****}P < 0.0001$. (*iv*) Representative confocal images of HUVECs treated with the indicated treatments. Live-cell cytoplasms were stained with Calcein-AM (green), and cell nuclei were stained with Hoechst (blue). Scale bar, 50 µm. (*C*) (*i*) Illustration of a cell culture well cross-section in the tube formation assay performed with GFP-expressing HUVECs that were applied with/without SC treatments. (*ii*) Whole-well representative images of GFP-expressing HUVECs imaged 18 h after seeding (*Top*) and the corresponding AngioTool software analysis images (*Bottom*). Scale bar, 1 mm. (*iii*) Computerized image analysis presents a significantly higher average vessel length in +FGF SC treatment than −FGF SCs and untreated control. Values were normalized to the untreated control values. The gray dot (+FGF SCs) represents an outlier. ($n = 8$ or 9). $^{**}P = 0.0014$; $^{****}P < 0.0001$. All results are presented as mean ± SD; n represents the number of independent samples in each group. One-way ANOVA with adjusted P value in multiple comparisons tests was used for statistical analysis. min to max, minimum to maximum; ns, not significant; Ex, Excitation; Em, Emission; Ec, Endothelial cell.

correlate with previous findings that indicated the role of FGF in maintaining vessel integrity (32, 33).

Interestingly, some tube formation was observed when SCs without DNA were applied to the natural cells. These results suggest a possible contribution of the SCs' components, such as essential nutrients (amino acids, nucleotides, energy supplements, lipids, etc.), in stimulating tube formation and elongation.

SCs Enhance the Formation of Stabilized Vascular Networks in Engineered Scaffolds. Growing mature blood vessels within engineered tissue constructs plays a crucial role in regenerative medicine, affecting the implant's proper integration and viability (34). Therefore, we assessed the ability of FGF-producing SCs to stimulate the development of a matured, three-dimensional vascular network in engineered tissue architectures. GFP-expressing HUVECs were cocultured with dental pulp stem cells (DPSCs) that support blood vessel formation and stabilization on CelGro collagen scaffolds (35). The cells were cultured for 1 wk, and FGF-producing SCs were exchanged every other day to maintain HUVEC viability, activating vessel self-assembly (Fig. 3*A* and *SI Appendix*, Fig. S9). The vessel coverage area and the total number of vessel junctions obtained after 7 d were significantly higher for the scaffolds applied with FGF-producing SCs relative to the other treatments (Fig. 3 *B*, *i–iii*). Surprisingly, FGF-SC treatment resulted in a more elongated and branched network than a purified TRX-FGF treatment that served as a positive control (*SI Appendix*, Fig. S10). In addition, similar to the two-dimensional tube assay (Fig. 2*C*), network self-assembly was obtained after applying the nonproducing SCs. However, this treatment was still significantly less effective than the FGF-producing SC treatment.

bFGF was reported to promote vessel maturation and stabilization of capillaries formed through physiological angiogenesis (32, 36). To examine the effect of FGF-producing SCs on vessel stabilization, we immunostained the whole mount of fixed constructs for vascular endothelial cadherin (VE-cadherin) as a vasculature indicator and collagen type IV as a characteristic marker of the basement membrane (34, 37). Three-dimensional images of the constructs analyzed using computational imaging demonstrated a twofold higher secretion volume of collagen-IV in the constructs treated with FGF SCs compared to controls (Fig. 3 *B*, *iv* and Movie S2). In addition, scaffolds were immunostained against α-smooth muscle actin, an element of vessel maturity, indicating the differentiation and attachment of mural cells to the forming vessels (38). Proangiogenic SCs also resulted in elongated supporting cells coating the forming capillaries (*SI Appendix*, Fig. S11), thus suggesting the SCs drive mural cell differentiation.

To better understand the effect of SCs on natural cells, we performed an antibody array against angiogenesis-related cytokines of cell media collected on day 7 after seeding the coculture (Fig. 3*C*). Elevated levels of VEGF-A, interleukin (IL)-6, and Epithelial-neutrophil activating peptide (ENA)-78 were detected, in addition to IL-8 and Monocyte chemotactic protein (MCP)-1, due to the presence of bFGF (39–42). In addition, we spotted low-level secretion of these cytokines in the samples treated with nonproducing SCs, which were consistently greater than the baseline levels (untreated control) but lower than those detected for FGF-producing SC treatments. In summary, proangiogenic SCs supported vascular formation and stabilization and altered endothelial-mural cell coculture cytokine secretion.

In situ Production of FGF by SCs Promotes In vivo Angiogenesis. To study the activity of proangiogenic SCs in situ, we utilized a Matrigel plug model in BALB/c mice (Fig. 4*A*). SCs were administrated subcutaneously into the mouse flank within a basement membrane–derived, factors-reduced gel matrix. One week later, we extracted the plugs, and visible differences in blood venule infiltration with increased invasion in the mice injected with the proangiogenic SCs were detected (Fig. 4 *B*, *i*). Hematoxylin and eosin (H&E) and anti-CD31 staining confirmed a significantly higher infiltration of endothelial cells and blood vessels toward plugs with proangiogenic SCs (Fig. 4 *B*, *ii* and *iii*). These findings indicate the in situ expression and release of human growth factors by SCs, leading to the activation of angiogenesis.

Systemic Immunogenicity of Locally Injected SCs. The in vivo immunogenic profile of SCs is a critical step in future clinical implementation. We assessed the immunogenic systemic response 1 wk after long exposure to the SCs in the Matrigel plug model. Blood samples were collected immediately after mice were euthanized and sent for complete blood count evaluation. Statistical analysis was used to assess the white blood cells (WBCs; count, neutrophils [%], lymphocytes [%], and monocytes [%]). Despite a relatively low neutrophil [%] count measured for mice treated with nonproducing SCs, the statistical data revealed no significant difference between the treatment groups (mice treated with FGF-producing SCs, nonproducing SCs, or vehicle control) for all tested values (Fig. 4*C*). In addition, visual inspection of the mice over treatment time did not reveal any discomfort or continual weight loss (*SI Appendix*, Fig. S12).

Discussion

As therapeutic compartments, SCs can provide some advantages that living cells simply cannot match, including their full engineerability, controllability, and versatile optional designs. Investigating the current capabilities and limitations of SCs to promote a complex morphogenetic physiological process within live tissues (e.g., angiogenesis) is essential for establishing their biomedical potential.

This study focuses on engineering proangiogenic SCs capable of autonomous production of recombinant human FGF with improved bioactivity under physiological conditions. Moreover, we show how proangiogenic SCs interact with living tissue, affecting neovascularization in vivo.

The SC's membrane composition plays an essential role in encapsulating a functional CFPS system and efficiently producing soluble proteins. Our findings demonstrate that a membrane composed of POPC and cholesterol resulted in favorable protein expression, confirmed further by ∼87% of active SCs in the total population, and high protein production, reaching $9{\cdot}10^6$ protein copies per cell. This result may be attributed to the influence of lipid composition on cell permeability and stability (39). Other studies have shown that fatty acid tail length and saturation as well as cholesterol concentration are all leading factors in tailoring these two properties (39–44). Membrane composition can also alter the resultant particle size (45). Our results suggest that the internal biochemical reaction volume, which affects molecular crowding, influences gene expression kinetics in synthetic cellular systems (28). Our findings show that incorporating POPC (having a hybrid 16:0 to 18:1 tail) with high cholesterol concentrations as membrane composition demonstrated improved SC activity compared to EPC, a natural PC lipid mixture formulated with the same amount of cholesterol. This observation was also true when comparing the POPC-SCs to a POPC:DOPC (18:1C lipid chain) mixture enriched with a lower cholesterol percentage. These results suggest that POPC-based SCs are superior to other lipids, balancing the formulation conditions and transcription and translation capabilities.

Optimizing the protein release mechanisms from SCs remains one of the future challenges for this field. According to our studies, the SC formulation presents a stable size distribution over 24 h, together with a decrease in protein concentrations inside the SCs over this period. However, the additional

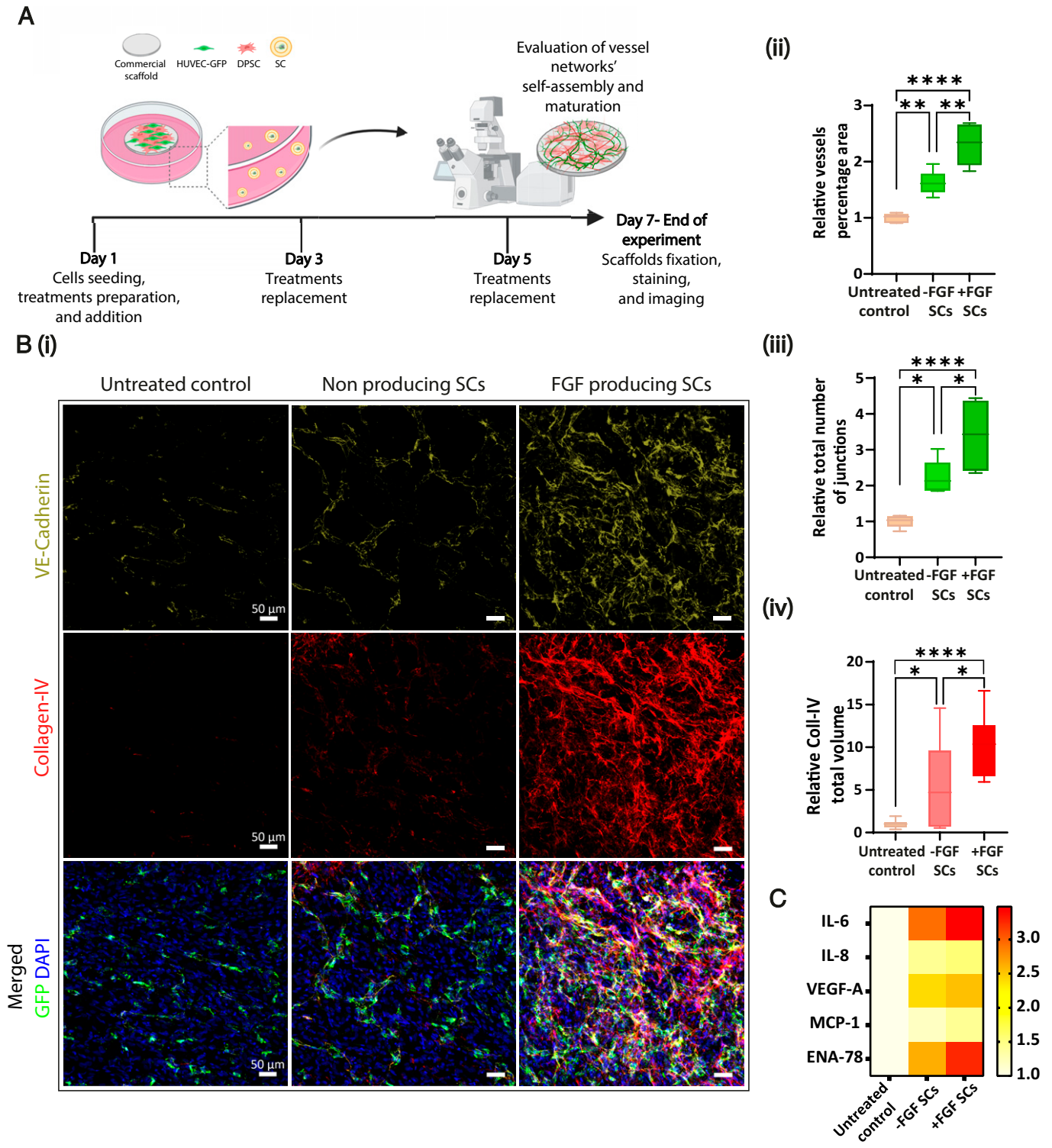

Fig. 3. Proangiogenic SCs drive the formation and stabilization of a three-dimensional vessel-like network. (*A*) DPSCs (in red) and HUVECs-GFP (in green) were coseeded on CelGro scaffolds with +/−FGF SCs or without treatment for 1 wk to test the formation of a three-dimensional vascular network. (*B*) (*i*) Representative maximum intensity projection confocal images of scaffolds fixed and immunostained for both VE-cadherin (green), endothelial cell marker, and Collagen-IV (Coll-IV, red), a main component of the basement membrane. Endogenously expressed GFP in HUVECs is marked in green. Cell nuclei were stained with DAPI (blue). Scale bar, 50 µm. (*ii*) Quantification of vessel area (%) and (*iii*) of the total number of junctions in the network shows better vasculature network properties in +FGF SCs treatment compared to controls ($n = 6$). *$P \leq 0.0231$; **$P \leq 0.0022$; ****$P < 0.0001$. (*iv*) Coll-IV total volume measured using the IMARIS surfaces module rendering shows approximately twofold higher Coll-IV secretion in +FGF SCs treatment compared to controls. All treatments were normalized to untreated control ($n = 3$). *$P \leq 0.0424$, ****$P < 0.0001$. Data are presented in box and whiskers displaying min to max plot and are expressed as mean ± SD; *n* is the number of independent samples in each group. One-way ANOVA with adjusted *P* value in multiple comparisons tests was used for statistical analysis. (*C*) Human angiogenesis-related cytokine secretion array was performed on conditioned media collected on day 7 of the experiment. The data presented in the heat map show increased cytokine secretion when cells were treated with the +FGF SCs. Coll-IV, Collagen-IV; min to max, minimum to maximum; MCP, Monocyte chemotactic protein; ENA, Epithelial-neutrophil activating peptide.

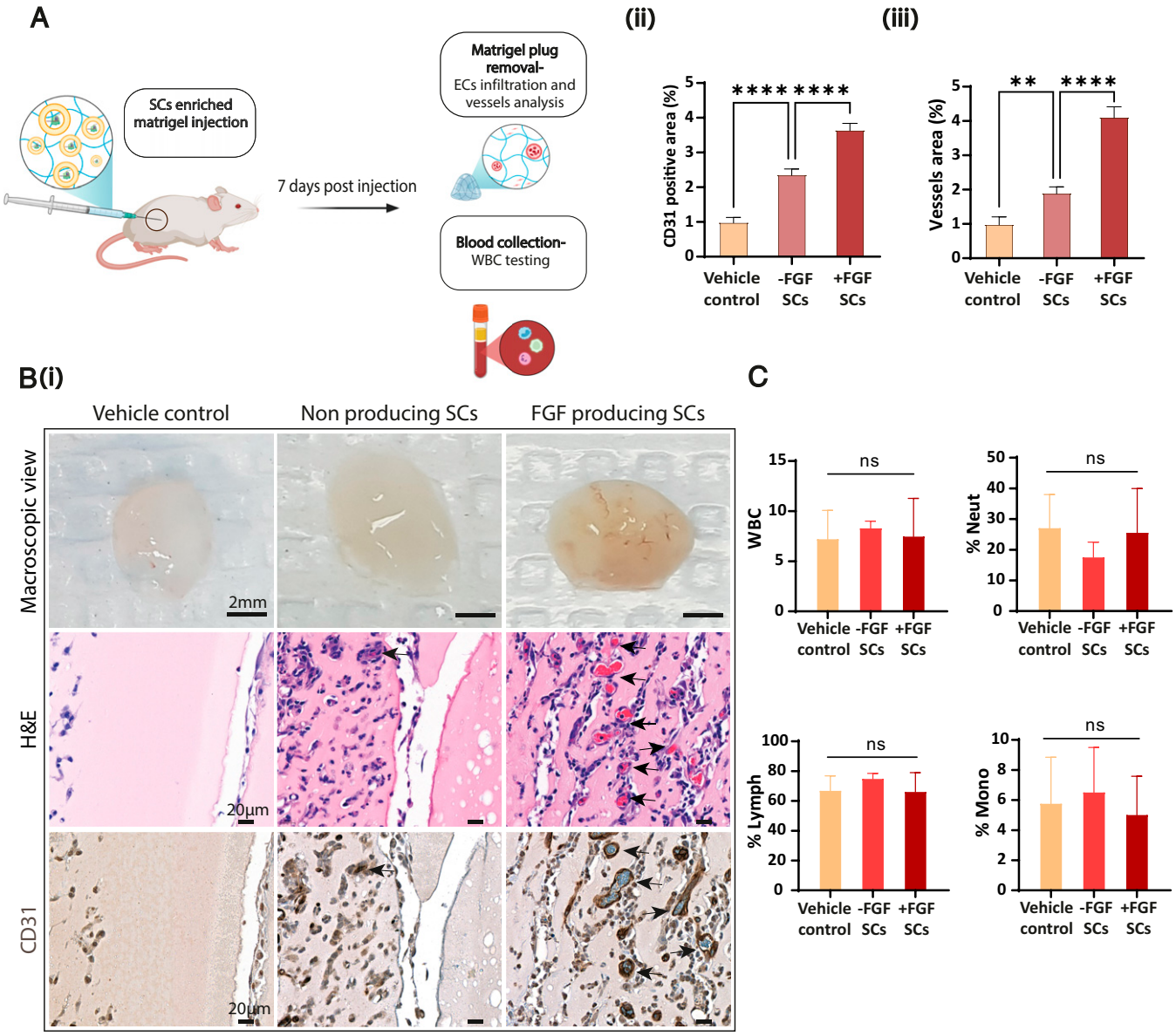

Fig. 4. In vivo integration of FGF-producing SCs increases endothelial cells and new capillaries infiltration toward Matrigel plugs. (*A*) BALB/c mice were subcutaneously injected with SCs (+/−FGF SCs) enriched growth factors–reduced Matrigel. PBS was used as assay control (vehicle control). Mice were killed 7 d after injection. (*B*) (*i*) Representative images of Matrigel plugs in macroscopic view, matching the indicated treatments (scale bar, 2 mm), of H&E-stained paraffin-embedded slides of the explanted plugs (scale bar, 20 µm), and the corresponding CD31 immunostained slides (scale bar, 20 µm). FGF-producing SC treatment shows increased convergence of newly formed blood vessels into the plug (arrows); EC, Endothelial cell. (*ii*) Quantification of CD31-expressing cells % area and (*iii*) vessels % area was assessed using CD31 immunostaining of plug sections. Results present mean ± SEM (n = 5 mice per treatment); $^{**}P = 0.0038$, $^{****}P < 0.0001$. (*C*) WBC count test of blood collected on day 7 of the experiment shows no significant difference between SC treatments and vehicle control. %Neut, %Neutrophils; %Lymph, %Lymphocytes; %Mono, %Monocytes of total WBC. Results present mean ± SD (n = 4 mice per treatment); ns = not significant. One-way ANOVA with adjusted P value in multiple comparisons tests was used for all statistical analyses.

results recorded at the same time range suggest protein release from the SCs due to membrane permeability. We hypothesize that protein release in the current SC formulation results from local membrane destabilization; this can be triggered by SC exposure to osmotic pressure differences or mechanical strains. From an evolutionary perspective, early cellular life forms may not have had sophisticated protein shuttling machinery, which evolved later in life (46, 47).

When designed with the optimized membrane and CFPS composition and a suitable genetic code, the proangiogenic SCs preserved prolonged growth factor production over 6 h. The levels of active FGF produced by the SCs were biologically sufficient to induce a diversity of angiogenesis-related cellular processes and associated-signaling pathways. Proangiogenic SCs biochemically interact with human endothelial cells, promoting their proliferation and survival, migration, and tubule-like formation. However, looking forward to their clinical realization, the development of active transfer of building blocks and energy self-regeneration mechanisms in SCs is still required to extend their life span.

The SCs induced basal vascular tube formation and angiogenic, proinflammatory cytokine secretion even without growth factor expression. A possible explanation for these results is that bacterial-based SCs expose bacterial components that can trigger an innate proinflammatory response (48). In addition, the SCs may provide necessary nutrients found in the CFPS system or the lipid membrane. Developments of nonbacterial cell-free systems can further reduce the off-target effects of the system. Yet, their reaction yields and their simplicity of preparation still need to be improved (49). Interestingly, the FGF-producing

SCs resulted in a higher angiogenic response than a purified protein treatment. Together, these data show an accumulative angiogenic effect delivered by the FGF-producing SC system.

We utilized the proangiogenic properties of the SCs to support neovascularization in engineered tissue constructs. Incubating the constructs with FGF-producing SCs facilitated the formation of stabilized vascular networks by affecting both endothelial and mural cells. This finding demonstrates that SCs can assist in supporting tissue rearrangement, which has high importance to a broad scope of research and therapeutic fields.

Finally, local integration of FGF-producing SCs in mice for prolonged periods of time (7 d) induced the recruitment of newly formed blood vessels toward gel plugs. Notable differences were recorded between the proangiogenic SC treatment with nonproducing SCs and vehicle control applications, indicating that angiogenesis was activated due to in situ production and release of the proangiogenic growth factor. In addition, the treatment did not induce detected side effects or immunogenic systemic response.

To summarize, this study demonstrates that protein-producing SCs can be integrated with live tissue to promote tissue remodeling. Synthetic biology tools such as SCs hold promise for revolutionizing biomedicine, such as drug delivery and tissue engineering.

Materials and Methods

Detailed *Materials and Methods* are provided in the *SI Appendix*. All illustrations and figures in this paper were created using BioRender.com and Adobe Illustrator. Chemical structures were illustrated using ChemDraw online.

Tube Formation Assay with SCs. To analyze the angiogenic activity of SCs, HUVECs-GFP were seeded at 10,000 cells/well on top of a growth factor–reduced basement membrane extract (GFR BME; 3445-005-01, R&D Systems)-coated Angiogenesis μ-Slide (Ibidi). The cells were applied with the same treatments mentioned in the proliferation assays section (*SI Appendix, Materials and Methods*) in a starvation M-199 medium (0.25% fetal bovine serum). The slide was incubated in humidified conditions, 37 °C and 5% CO_2, inside the Lionheart FX automated microscope system (Agilent) for 18 h, and the different wells were constantly imaged. The level of tube structure formation was quantified via the AngioTool analysis software, as described in the published user manual (31). All treatments were normalized to the average value of untreated cell control in the same experimental repeat.

Matrigel Plug Model with SCs. All animal studies were approved by the institutional and ethical committee at Technion (Haifa, Israel). An adapted Matrigel plug model (50) in BALB/c mice was used to assess the in vivo activity of proangiogenic SCs. Six-week-old female mice were anesthetized, and 500 μL liquid GFR BME (3445-005-01, R&D Systems) enriched with 20% vol/vol of SCs (with/without FGF DNA) or with phosphate-buffered saline (PBS) only and supplemented with Heparin (0.1 mg/mL; Sciencell) were subcutaneously injected into their flank. The SCs were kept on ice before injection to ensure in situ protein production. The mice were killed 7 d after injection, and the Matrigel plugs were removed for imaging and analysis.

Statistics. The statistical analysis, including Student's *t* test and one-way ANOVA, was performed using Prism GraphPad version 9.3.1.

Data, Materials, and Software Availability. Supplementary study data are available online and from the corresponding author upon reasonable request. The codes used in this study for image analysis are available at Zenodo https://zenodo.org/record/7029622 (51).

All study data are included in the article and/or supporting information.

ACKNOWLEDGMENTS. This work was supported by the European Union's Horizon 2020 research and innovation program under grant agreement No. 680242-ERC-[Next-Generation Personalized Diagnostic Nanotechnologies for Predicting Response to Cancer Medicine]. We also acknowledge the support of the Israel Innovation Authority for the Nofar Grant (67967), The Israel Ministry of Economy for a Kamin Grant (52752, 69230); the Israel Science Foundation (1778/13, 1421/17); the Israel Ministry of Science, Technology & Space (3-16963; 3-17418); the Ministry of Agriculture & Rural Development - Office of the Chief Scientist (323/19); the Israel Cancer Association (2015-0116); the Leventhal 2020 COVID19 Research Fund (ATS #11947), the German-Israeli Foundation for Scientific Research and Development for a German-Israeli Foundation (GIF) Young grant (I-2328-1139.10/2012); the European Union FP-7 International Reintegration Grants (IRG) Program for a Career Integration Grant (908049); the Phospholipid Research Center Grant (ASC-2018-062/1-1); the Louis family Cancer Research Fund; a Mallat Family Foundation Grant; the Unger Family Fund; a Carrie Rosenblatt Cancer Research Fund; the Technion Integrated Cancer Center (TICC); the Russell Berrie Nanotechnology Institute; and the Lorry I. Lokey Interdisciplinary Center for Life Sciences & Engineering. A.S. acknowledges Alon and Taub Fellowships. G.C. wishes to thank the Baroness Ariane de Rothschild Women Doctoral Program from the Rothschild Caesarea Foundation and The National Forum for Bio-Innovators by TEVA Pharmaceuticals for the Doctoral Fellowship. M.K. acknowledges the TICC Rubinstein scholarship and Robert B. Kalmansohn Fellowship Fund in the Emerson Life Sciences Building. O.A. acknowledges Jacobs and Gutwirth Fellowships. In addition, we wish to thank Dr. Yael Lupu-Haber and Dr. Nitzan Dahan from the Lorry I. Lokey Interdisciplinary Center for Life Sciences & Engineering and Dr. Hüseyin Tuncay from Biotek (Agilent) for assisting in creating microscopy protocols and guidance through their analysis. We also wish to thank Yael Shammai for contributing to the in vivo experiments.

Author affiliations: [a]The Luis Family Laboratory for Targeted Drug Delivery and Personalized Medicine Technologies, Department of Chemical Engineering, Technion, Haifa 32000, Israel; [b]The Interdisciplinary Program for Biotechnology, Technion, Haifa 32000, Israel; [c]Department of Biomedical Engineering, Technion, Haifa 32000, Israel; [d]The Norman Seiden Multidisciplinary Program for Nanoscience and Nanotechnology, Technion, Haifa 32000, Israel; and [e]The Ruth and Bruce Rappaport Faculty of Medicine, Technion, Haifa 31096, Israel

1. K. Göpfrich, I. Platzman, J. P. Spatz, Mastering complexity: Towards bottom-up construction of multifunctional eukaryotic synthetic cells. *Trends Biotechnol.* **36**, 938–951 (2018).
2. V. Noireaux, A. Libchaber, A vesicle bioreactor as a step toward an artificial cell assembly. *Proc. Natl. Acad. Sci. U.S.A.* **101**, 17669–17674 (2004).
3. Ö. D. Toparlak *et al.*, Artificial cells drive neural differentiation. *Sci. Adv.* **6**, eabb4920 (2020).
4. Y. Elani, R. V. Law, O. Ces, Protein synthesis in artificial cells: Using compartmentalisation for spatial organisation in vesicle bioreactors. *Phys. Chem. Chem. Phys.* **17**, 15534–15537 (2015).
5. P. van Nies *et al.*, Self-replication of DNA by its encoded proteins in liposome-based synthetic cells. *Nat. Commun.* **9**, 1583 (2018).
6. K. P. Adamala, D. A. Martin-Alarcon, K. R. Guthrie-Honea, E. S. Boyden, Engineering genetic circuit interactions within and between synthetic minimal cells. *Nat. Chem.* **9**, 431–439 (2017).
7. O. Adir *et al.*, Synthetic cells with self-activating optogenetic proteins communicate with natural cells. *Nat. Commun.* **13**, 2328 (2022).
8. W. Sato, T. Zajkowski, F. Moser, K. P. Adamala, Synthetic cells in biomedical applications. *Wiley Interdiscip. Rev. Nanomed. Nanobiotechnol.* **14**, e1761 (2022).
9. M. H. M. E. Stevendaal, J. C. M. Hest, A. F. Mason, Functional interactions between bottom-up synthetic cells and living matter for biomedical applications. *ChemSystemsChem* **3**, e2100009 (2021).
10. Z. Chen *et al.*, Synthetic beta cells for fusion-mediated dynamic insulin secretion. *Nat. Chem. Biol.* **14**, 86–93 (2018).
11. V. Mukwaya, S. Mann, H. Dou, Chemical communication at the synthetic cell/living cell interface. *Commun. Chem.* **4**, 161 (2021).
12. J. Liu *et al.*, Genetically encoded synthetic beta cells for insulin biosynthesis and release under hyperglycemic conditions. *Adv. Funct. Mater.* **32**, 2111271 (2022).
13. N. Krinsky *et al.*, Synthetic cells synthesize therapeutic proteins inside tumors. *Adv. Healthc. Mater.* **7**, e1701163 (2018).
14. M. Potente, H. Gerhardt, P. Carmeliet, Basic and therapeutic aspects of angiogenesis. *Cell* **146**, 873–887 (2011).
15. C. Tapeinos, H. Gao, T. Bauleth-Ramos, H. A. Santos, Progress in stimuli-responsive biomaterials for treating cardiovascular and cerebrovascular diseases. *Small*, 10.1002/smll.202200291 (2022).
16. R. Subbiah, R. E. Guldberg, Materials science and design principles of growth factor delivery systems in tissue engineering and regenerative medicine. *Adv. Healthc. Mater.* **8**, e1801000 (2019).
17. A. Wieslander, A. Christiansson, L. Rilfors, G. Lindblom, Lipid bilayer stability in membranes. Regulation of lipid composition in *Acholeplasma laidlawii* as governed by molecular shape. *Biochemistry* **19**, 3650–3655 (1980).
18. O. Adir *et al.*, Preparing protein producing synthetic cells using cell free bacterial extracts, liposomes and emulsion transfer. *J. Vis. Exp.* **158**, e60829 (2020).
19. W. W. Sułkowski, D. Pentak, K. Nowak, A. Sułkowska, The influence of temperature, cholesterol content and pH on liposome stability. *J. Mol. Struct.* **744–747**, 737–747 (2005).
20. Y. Shimizu *et al.*, Cell-free translation reconstituted with purified components. *Nat. Biotechnol.* **19**, 751–755 (2001).

21. A. Moga, N. Yandrapalli, R. Dimova, T. Robinson, Optimization of the inverted emulsion method for high-yield production of biomimetic giant unilamellar vesicles. *ChemBioChem* **20**, 2674–2682 (2019).
22. Y. R. Yun *et al.*, Fibroblast growth factors: Biology, function, and application for tissue regeneration. *J. Tissue Eng.* **2010**, 218142 (2010).
23. N. Ferrara, H.-P. Gerber, J. LeCouter, The biology of VEGF and its receptors. *Nat. Med.* **9**, 669–676 (2003).
24. D. M. Ornitz, N. Itoh, Fibroblast growth factors. *Genome Biol.* **2**, REVIEWS3005 (2001).
25. Y. Xie *et al.*, FGF/FGFR signaling in health and disease. *Signal Transduct. Target. Ther.* **5**, 181 (2020).
26. J. Wang *et al.*, Biochemical properties of C78SC96S rhFGF-2: A double point-mutated rhFGF-2 increases obviously its activity. *J. Biotechnol.* **121**, 442–447 (2006).
27. M. E. Gasparian *et al.*, Overexpression in *Escherichia coli* and purification of human fibroblast growth factor (FGF-2). *Biochemistry (Mosc.)* **74**, 221–225 (2009).
28. C. Tan, S. Saurabh, M. P. Bruchez, R. Schwartz, P. Leduc, Molecular crowding shapes gene expression in synthetic cellular nanosystems. *Nat. Nanotechnol.* **8**, 602–608 (2013).
29. Q. M. Nunes, Y. Li, C. Sun, T. K. Kinnunen, D. G. Fernig, Fibroblast growth factors as tissue repair and regeneration therapeutics. *PeerJ* **4**, e1535 (2016).
30. I. Arnaoutova, J. George, H. K. Kleinman, G. Benton, The endothelial cell tube formation assay on basement membrane turns 20: State of the science and the art. *Angiogenesis* **12**, 267–274 (2009).
31. E. Zudaire, L. Gambardella, C. Kurcz, S. Vermeren, A computational tool for quantitative analysis of vascular networks. *PLoS One* **6**, e27385 (2011).
32. J. Welti, S. Loges, S. Dimmeler, P. Carmeliet, Recent molecular discoveries in angiogenesis and antiangiogenic therapies in cancer. *J. Clin. Invest.* **123**, 3190–3200 (2013).
33. M. Murakami, Signaling required for blood vessel maintenance: Molecular basis and pathological manifestations. *Int. J. Vasc. Med.* **2012**, 293641 (2012).
34. S. Ben-Shaul, S. Landau, U. Merdler, S. Levenberg, Mature vessel networks in engineered tissue promote graft-host anastomosis and prevent graft thrombosis. *Proc. Natl. Acad. Sci. U.S.A.* **116**, 2955–2960 (2019).
35. S. Landau *et al.*, Investigating lymphangiogenesis in vitro and in vivo using engineered human lymphatic vessel networks. *Proc. Natl. Acad. Sci. U.S.A.* **118**, e2101931118 (2021).
36. M. Murakami, M. Simons, Fibroblast growth factor regulation of neovascularization. *Curr. Opin. Hematol.* **15**, 215–220 (2008).
37. M. Paulsson, Basement membrane proteins: Structure, assembly, and cellular interactions. *Crit. Rev. Biochem. Mol. Biol.* **27**, 93–127 (1992).
38. R. Cao *et al.*, Angiogenic synergism, vascular stability and improvement of hind-limb ischemia by a combination of PDGF-BB and FGF-2. *Nat. Med.* **9**, 604–613 (2003).
39. K. A. Podolsky, N. K. Devaraj, Synthesis of lipid membranes for artificial cells. *Nat. Rev. Chem.* **5**, 676–694 (2021).
40. J. F. Nagle, J. C. Mathai, M. L. Zeidel, S. Tristram-Nagle, Theory of passive permeability through lipid bilayers. *J. Gen. Physiol.* **131**, 77–85 (2008).
41. J. De Gier, J. G. Mandersloot, L. L. M. Van Deenen, Lipid composition and permeability of liposomes. *Biochim. Biophys. Acta* **150**, 666–675 (1968).
42. F. Caschera, J. W. Lee, K. K. Ho, A. P. Liu, M. C. Jewett, Cell-free compartmentalized protein synthesis inside double emulsion templated liposomes with in vitro synthesized and assembled ribosomes. *Chem. Commun. (Camb.)* **52**, 5467–5469 (2016).
43. M. C. Blok, E. C. van der Neut-Kok, L. L. van Deenen, J. de Gier, The effect of chain length and lipid phase transitions on the selective permeability properties of liposomes. *Biochim. Biophys. Acta* **406**, 187–196 (1975).
44. K. Nishimura *et al.*, Identification of giant unilamellar vesicles with permeability to small charged molecules. *RSC Advances* **4**, 35224 (2014).
45. P. C. Soema, G. J. Willems, W. Jiskoot, J. P. Amorij, G. F. Kersten, Predicting the influence of liposomal lipid composition on liposome size, zeta potential and liposome-induced dendritic cell maturation using a design of experiments approach. *Eur. J. Pharm. Biopharm.* **94**, 427–435 (2015).
46. A. Y. Mulkidjanian, M. Y. Galperin, E. V. Koonin, Co-evolution of primordial membranes and membrane proteins. *Trends Biochem. Sci.* **34**, 206–215 (2009).
47. B. Bertrand, R. Garduño-Juárez, C. Munoz-Garay, Estimation of pore dimensions in lipid membranes induced by peptides and other biomolecules: A review. *Biochim. Biophys. Acta Biomembr.* **1863**, 183551 (2021).
48. M. H. G. Z. Ho, Z. M. Guo, J. Chunga, J. S. Goodwin, H. Xie, Characterization of innate immune responses of human endothelial cells induced by *Porphyromonas gingivalis* and their derived outer membrane vesicles. *Front. Cell. Infect. Microbiol.* **6**, 139 (2016).
49. A. Zemella, L. Thoring, C. Hoffmeister, S. Kubick, Cell-free protein synthesis: Pros and cons of prokaryotic and eukaryotic systems. *ChemBioChem* **16**, 2420–2431 (2015).
50. P. Kastana *et al.*, *Matrigel Plug Assay for In vivo Evaluation of Angiogenesis* (Springer New York, 2019), pp. 219–232.
51. G. Chen, O. Adir, A. Schroeder, Implanted synthetic cells trigger tissue angiogenesis through de novo production of recombinant growth factors. Zenodo. https://zenodo.org/record/7029622. Deposited 28 August 2022.